AGU PUBLICATIONS

Geophysical Research Letters

RESEARCH LETTER
10.1002/2014GL060219

**Key Points:**
- Deformation of atmospheric organic particles investigated with X-ray microscopy
- Extent of deformation is related to viscosity and surface tension of particles
- Deformation of ambient and laboratory-generated particles are compared

**Supporting Information:**
- Readme
- Text S1
- Figure S1
- Figure S2
- Figure S3
- Figure S4
- Figure S5
- Table S1
- Table S2
- Table S3
- Table S4
- Table S5

**Correspondence to:**
R. E. O'Brien,
resellon@lbl.gov

**Citation:**
O'Brien, R. E., A. Neu, S. A. Epstein, A. C. MacMillan, B. Wang, S. T. Kelly, S. A. Nizkorodov, A. Laskin, R. C. Moffet, and M. K. Gilles (2014), Physical properties of ambient and laboratory-generated secondary organic aerosol, *Geophys. Res. Lett.*, *41*, 4347–4353, doi:10.1002/2014GL060219.

Received 11 APR 2014
Accepted 28 MAY 2014
Accepted article online 2 JUN 2014
Published online 17 JUN 2014

# Physical properties of ambient and laboratory-generated secondary organic aerosol

**Rachel E. O'Brien[1,2], Alexander Neu[1], Scott A. Epstein[3], Amanda C. MacMillan[3], Bingbing Wang[4], Stephen T. Kelly[1], Sergey A. Nizkorodov[3], Alexander Laskin[4], Ryan C. Moffet[2], and Mary K. Gilles[1]**

[1]Chemical Sciences Division, Lawrence Berkeley National Laboratory, Berkeley, California, USA, [2]Department of Chemistry, University of the Pacific, Stockton, California, USA, [3]Department of Chemistry, University of California, Irvine, California, USA, [4]William R. Wiley Environmental and Molecular Sciences Laboratory, Pacific Northwest National Laboratory, Richland, Washington, USA

**Abstract** The size and thickness of organic aerosol particles collected by impaction in five field campaigns were compared to those of laboratory-generated secondary organic aerosols (SOA). Scanning transmission X-ray microscopy was used to measure the total carbon absorbance (TCA) by individual particles as a function of their projection areas on the substrate. Particles with higher viscosity/surface tension can be identified by a steeper slope on a plot of TCA versus size because they flatten less upon impaction. The slopes of the ambient data are statistically similar indicating a small range of average viscosities/surface tensions across five field campaigns. Steeper slopes were observed for the plots corresponding to ambient particles, while smaller slopes were indicative of the laboratory-generated SOA. This comparison indicates that ambient organic particles have higher viscosities/surface tensions than those typically generated in laboratory SOA studies.

## 1. Introduction

Organic aerosols constitute a significant fraction of atmospheric fine mode particulate matter [*Zhang et al.*, 2007]. Models of secondary organic aerosol (SOA) formation and aging assume that SOA consists of liquid particles with condensed phase diffusion rates that are fast enough to maintain equilibrium with the gas phase [*Pankow*, 1994; *Hallquist et al.*, 2009]. However, recent studies examining particle bounce behavior [*Virtanen et al.*, 2010], response to physical manipulation [*Renbaum-Wolff et al.*, 2013], evaporation [*Vaden et al.*, 2011; *Abramson et al.*, 2013; *Loza et al.*, 2013], thermal desorption [*Cappa and Wilson*, 2011], particulate nitrate uptake [*Perraud et al.*, 2012], ammonia uptake [*Kuwata and Martin*, 2012], phase state [*Wang et al.*, 2012], and diffusion [*Vaden et al.*, 2010] provide evidence that both laboratory and ambient particles can have higher viscosities. The phase state of organic aerosols, whether solid/amorphous solid (higher viscosity) or liquid (lower viscosity), is not well understood. Most studies have been done on small sample sizes with little intercomparison across ambient samples, and only a few studies [*Virtanen et al.*, 2010; *Vaden et al.*, 2011] compared laboratory and ambient samples. An investigation of the viscosity of particles from different geographical locations and under a range of conditions provides an opportunity to examine existing assumptions about chemical composition and kinetics and to constrain the range of viscosity values appropriate for SOA models.

When an aerosol particle impacts a surface, some kinetic energy is dissipated in deformation. If the kinetic energy loss is large enough that the adhesion energy exceeds the rebound energy, then the particle will remain on the surface. The viscosity, including both elastic properties and liquid flow properties [*Ivosevic et al.*, 2006], as well as the surface tension (liquid vapor and liquid substrate), determine both the adhesion probability and the final shape of the impacted particle. In this work, we compare the size and thickness of the impacted particles measured by scanning transmission X-ray microscopy/near-edge X-ray absorption fine structure (STXM/NEXAFS) in order to assess the extent of particle deformation and to provide useful information on particle properties.

## 2. Experimental

Ambient aerosols were collected over five field campaigns between 2001 and 2010. Figure 1 shows the geographic locations of these field sites. All of the campaigns were in North and South America. Two were in


**Figure 1.** Map showing the geographic locations of the five field campaigns. Samples from the VOCALS campaign in Chile and the NAOPEX campaign in the Boston area were aerial samples; MILAGRO, CARES, and YACS samples were collected at the ground sites.

California: Carbonaceous Aerosols and Radiative Effects Study (CARES) (2010) in the Sacramento Valley [*Zaveri et al.*, 2012] and Yosemite Aerosol Characterization Study (YACS) (2002) in Yosemite National Park [*Hand et al.*, 2005]. The Nighttime Aerosol/Oxidant Plume Experiment (NAOPEX) campaign (2001) [*Zaveri et al.*, 2010], Megacity Initiative: Local and Global Research Observations (MILAGRO) campaign (2006) [*Molina et al.*, 2010], and Variability of the American Monsoon Systems Ocean-Cloud-Atmosphere-Land Study (VOCALS) (2008) [*Wood et al.*, 2011] took place in the Boston area, the Mexico City metropolitan area, and Chile, respectively.

Laboratory samples were generated using a 5 $m^3$ Teflon chamber with UV-B broadband lamps in the absence of inorganic seed particles [*Nguyen et al.*, 2011b]. All chamber experiments were done in a dry chamber (relative humidity (RH) $<$ 2% at room temperature) that was flushed overnight with dry air between experiments. The isoprene SOA samples had ~100 μl $H_2O_2$ (Aldrich, 30% by volume in water) injected into a glass bulb and evaporated into the chamber with dry air followed by a similar injection and evaporation of ~20 μl isoprene (Aldrich, 99% purity). The starting mixing ratios of isoprene and $H_2O_2$ were 1 ppm and 6 ppm, respectively. For the high $NO_x$ (*h*-$NO_x$) experiments, a small, controlled volume of gas from a NO cylinder (Praxair, 5000 ppm NO in $N_2$) was injected in the chamber. For the *h*-$NO_x$ experiment, the initial mixing ratios of NO and $NO_y$ were ~400 and 500 ppb, respectively; the $NO_x$ level was below the detection limit (2 ppb) in the low-$NO_x$ (*l*-$NO_x$) experiments. Photo-oxidation times were 2–3 h. Limonene SOA was generated by injecting *d*-limonene (10 μl → 300 ppb) and ozone (~600 ppb) into the dry, dark chamber. Additional samples were prepared using a flow tube [*Bones et al.*, 2010]. Either *d*-limonene or $\alpha$-pinene was introduced into a flow of zero air ($H_2O$, $CO_2$, and volatile organic compounds (VOCs) removed) and dry ozone using a syringe pump at liquid flow rates of 16 and 25 μl/h, respectively. Additional information on particle generation and instrumentation is provided in the supporting information.

Ambient samples were collected using a TRAC (time-resolved aerosol collector) sampler with an effective cutoff size, $d_{50}$, of 0.36–0.38 μm [*Laskin et al.*, 2006]. Copper-grid-supported carbon B films and silicon nitride ($Si_3N_4$)-coated Si frames were used as impaction substrates. Both substrates have a similar hydrophobicity; bench top tests with ~15–20 μl droplets of Millipore water resulted in contact angles between 60–62° for the Si3N4 windows and 55–60° for the carbon B films. Therefore, minimal differences in impaction behavior are expected between the two substrates. Laboratory samples were collected on the seventh and eighth stages of a rotating MOUDI (multiorifice uniform-deposit impactor, MSP 110-R) with aerodynamic cutoff points of 0.32 μm and 0.18 μm, respectively [*Marple et al.*, 1991] using $Si_3N_4$-coated Si frames as substrates. The impactor RH is equal to the product of the ambient RH and the ratio of the impactor pressure to the ambient pressure [*Saukko et al.*, 2012]. Since the pressure at the MOUDI's seventh and eighth stages is 95% and 89% of the inlet pressure, the particles experience minor changes in RH during impaction. For the TRAC, the pressure in the sampling area is 70% of the ambient pressure, but the ~30 μs spent in the impaction region (between the nozzle and the impaction surface) is insufficient for equilibration of the ~300–400 nm aerodynamic diameter particles with respect to the water loss prior to impaction [*Koop et al.*, 2011; *Saukko et al.*, 2012].

Since the samples remain in the reduced pressure region after impaction, for the duration of the sampling time, loss of higher volatility compounds is likely. The amount of loss may be sample dependent, and this is a potential source of scatter in the data as well as systematic error.

In the TRAC sampler the particle impaction velocity is ~90 m/s [*Laskin et al.*, 2006]. In the MOUDI the velocity is ~36 m/s and ~87 m/s on stages 7 and 8, respectively [*Marple et al.*, 1991]. Therefore, any comparison between the samples collected with these two techniques must take into account that, due to the difference in impaction velocities, identical particles collected in the field studies using the TRAC will deform more than similar particles collected on stage 7 of the MOUDI.

STXM/NEXAFS measurements were taken at the Advanced Light Source at Lawrence Berkeley National Laboratory on beamlines 11.0.2 and 5.3.2.2. The operation of the microscope has been explained in detail by *Kilcoyne et al.* [2003]. Briefly, samples were held at the focal point (30–40 nm spot size) and raster scanned. Transmitted X-rays were detected, the X-ray photon energy was incremented, and images at four energies (278, 285.4, 288, and 320 eV) were collected. The work presented here uses analysis of images collected at the carbon K-edge, focusing on 278 and 320 eV. These energies correspond to absorbance due to the carbon preedge and postedge, respectively [*Henke et al.*, 1993; *Moffet et al.*, 2010a]. The STXM measurements were performed after an initial pump down to ~100 mTorr followed by a backfill with He to 20 Torr.

STXM/NEXAFS data were imported into MATLAB software for further analysis [*Moffet et al.*, 2010a]. The pixels determined to contain particles were assigned an intensity value ($I$), the particle-free pixels were assigned a background intensity value ($I_0$), and the absorbance or optical density (OD) was calculated via equation (1)

$$\mathrm{OD} = -\ln(I/I_0) = \mu\rho d \quad (1)$$

where $\mu$ is the mass absorption coefficient ($cm^2/g$), $\rho$ is the density ($g/cm^3$), and $d$ is the thickness of the particle (cm). By examining the difference in OD between the postedge and the preedge, the total carbon absorbance (TCA) can be calculated according to equation (2) (subscripts correspond to the X-ray photon energies) [*Moffet et al.*, 2011] as follows:

$$\mathrm{TCA} = \mathrm{OD}_{320}\text{-}\mathrm{OD}_{278} \quad (2)$$

TCA is calculated as an average over each particle and is proportional to the average number of carbon atoms in the particle [*Henke et al.*, 1993]. Assuming similar densities and similar mass absorption coefficients, an organic aerosol particle with larger TCA per unit area is a thicker particle.

Three component types were identified: organic, inorganic, and elemental carbon (soot) following the techniques of *Moffet et al.* [2010a]. Briefly, pixels in particles with positive values for TCA were assigned as organic, pixels with $OD_{278}/OD_{320}$ greater than 0.5 were assigned as inorganic, and pixels with the contribution of $sp^2$ carbon greater than 35% were assigned as soot [*Moffet et al.*, 2010a]. Only particles identified as predominantly organic, without any inorganic dominant regions and/or inclusions and without soot inclusions, were selected for the data sets presented in this manuscript. Some particles were likely nonspherical and had noncircular impaction areas; hence, the sizes are reported as area equivalent diameters. The supporting information contains additional information on the data collection and analysis. In this manuscript, the phrase "particle" and "aerosol particle" will both be used to refer to the particles in laboratory-generated and ambient aerosols.

## 3. Results and Discussion

Figure 2 displays the linear fit lines for the TCA values versus the size of impacted particles for all data sets. The data sets for the ambient and laboratory-generated particles are shown with solid lines and dashed lines, respectively. A steeper slope indicates that the particles have flattened less during impaction and thus likely have a higher viscosity/surface tension. Plots of individual particle measurements in all data sets and corresponding fitting parameters are provided in Table 1 and Figures S1 and S2 in the supporting information. SEM images showing the shapes of representative particles from laboratory and ambient samples are provided in Figure S3. The red and blue shaded areas highlight the range of the 95% confidence intervals for the ambient and laboratory particles, respectively. The slopes of four of the ambient data sets fall within the 95% confidence intervals of the other ambient data sets, consistent with similar viscosities/surface

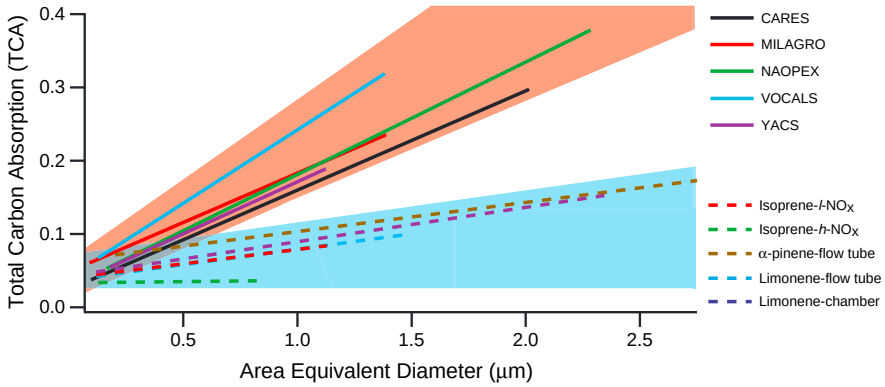


**Figure 2.** Optical thickness of carbon (total carbon absorption) as a function of size of the impacted organic particles. Solid and dashed lines: linear fit lines for the ambient and laboratory-generated particles, respectively. The red and blue areas highlight the range of the ±95% confidence intervals for the ambient and laboratory samples, respectively. *l*-$NO_x$ and *h*-$NO_x$ refer to samples generated from oxidation of OH under low-$NO_x$ and high-$NO_x$ conditions; ozone is used as the oxidant for the remaining samples.

tensions between the samples. The VOCALS data set is slightly outside the confidence intervals for the CARES and MILAGRO data sets but within the confidence intervals of the other two. This similarity indicates that a small range of viscosity/surface tension values may adequately describe the average aerosol population used in SOA models.

In Figure 2, all of the laboratory samples have smaller slopes than the ambient samples. Since most of the laboratory particles were collected on the seventh stage of a MOUDI which, as discussed above, has a smaller impaction velocity than the TRAC, the difference in physical properties between the ambient and laboratory samples is likely even larger than what was observed here. Four of the laboratory samples' slopes lie within the 95% confidence intervals of the others. Thus, the different oxidants, precursors, and different conditions (chamber versus flow tube) used in those samples have minimal effect on the viscosities/surface tensions of the aerosols formed. The isoprene sample generated under *h*-$NO_x$ conditions is the outlier, outside the 95% confidence intervals of the other samples, with a slope that is about 1 order of magnitude smaller than the other lab samples. The smaller slope arises because the slope of $OD_{278}$ versus size is slightly lower than, but within the 95% confidence interval, of the $OD_{320}$ slope (Table S2). Preedge absorbance ($OD_{278}$) arises from absorption and scattering by noncarbon atoms such as nitrogen, oxygen, sulfur, etc. Postedge absorbance ($OD_{320}$) is due to absorption and scattering from carbon as well as the other atoms. Photooxidation of isoprene under *h*-$NO_x$ conditions is known to generate compounds with higher O/C ratio and significant nitrogen content compared to the *l*-$NO_x$ conditions [*Nguyen et al.*, 2011a]. However, since the slope of the $OD_{320}$ versus size is lower than and outside the 95% confidence intervals of the other laboratory samples (Table S2), the scattering and absorption by the heteroatoms does not fully account for the smaller slope for the *h*-$NO_x$ sample, which means that the particles have flattened more on the substrate and likely have a lower viscosity/surface tension than the other laboratory samples. Potential reasons for this difference include the following: (1) isoprene particles formed under *h*-$NO_x$ conditions and under *l*-$NO_x$ conditions have different chemical

**Table 1.** Ambient and Laboratory Fitting Results for TCA Versus Size[a]

| Campaign | Slope | Intercept | Sample | Slope | Intercept |
|---|---|---|---|---|---|
| CARES | 0.14 ± 0.005 | 0.024 ± 0.003 | Isoprene-*l*-$NO_x$ | 0.039 ± 0.004 | 0.040 ± 0.002 |
| MILAGRO | 0.13 ± 0.01 | 0.048 ± 0.005 | Isoprene-*h*-$NO_x$ | 0.0036 ± 0.009 | 0.033 ± 0.004 |
| NAOPEX | 0.15 ± 0.02 | 0.028 ± 0.01 | α-pinene-flow tube | 0.040 ± 0.008 | 0.063 ± 0.009 |
| VOCALS | 0.20 ± 0.04 | 0.042 ± 0.02 | Limonene-flow tube | 0.042 ± 0.008 | 0.037 ± 0.005 |
| YACS | 0.14 ± 0.02 | 0.029 ± 0.01 | Limonene-chamber | 0.047 ± 0.006 | 0.043 ± 0.005 |

[a]The ±95% confidence intervals for the slope and intercept are given.

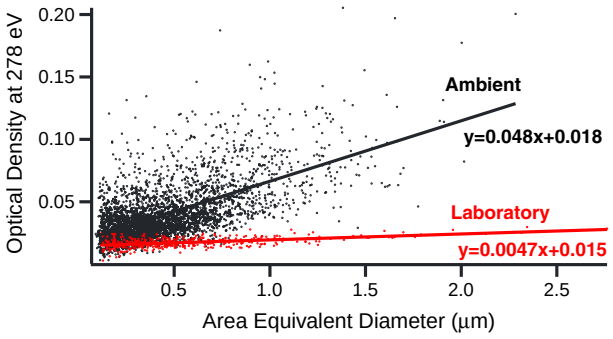


**Figure 3.** Optical density at 278 eV (preedge) versus particle size (area equivalent diameter). Black: all ambient samples and red: all laboratory samples. The best fit lines and equations are shown for each data set.

compositions [*Nguyen et al.*, 2011a] and (2) the *h*-$NO_x$ aerosols formed more quickly and were in the chamber for a shorter period of time (~2 h for *h*-$NO_x$ versus ~3 h for the *l*-$NO_x$ experiments).

The difference between ambient and laboratory particles is consistent with observations of slower evaporation kinetics for ambient SOA compared to laboratory-generated SOA [*Vaden et al.*, 2011]. However, *Virtanen et al.* [2010] reported a higher bounce fraction for chamber SOA than that for atmospheric SOA which is consistent with higher viscosity/more glassy (amorphous solid) particles in their chamber compared to the ambient. It is important to note that their chamber SOA was generated from a mixture of all of the volatile organic compounds (VOCs) emitted by pine seedlings. Thus, the differences between our results and the results of Virtanen could be due to our laboratory experiments using a single VOC precursor rather than a complex mixture.

A variety of techniques have indicated that laboratory-generated particles are amorphous semisolid particles [*Vaden et al.*, 2010; *Virtanen et al.*, 2010; *Cappa and Wilson*, 2011; *Vaden et al.*, 2011; *Kuwata and Martin*, 2012; *Perraud et al.*, 2012]. In contrast, the data from this study show that the laboratory-generated particles have smaller slopes than the ambient particles. The analysis presented here examines deformation behavior of particles upon impaction. Since deformation depends upon both viscosity and surface tension, a direct comparison between the relative extent of deformation observed here and the viscosities reported in other studies should be made with caution. However, the laboratory conditions used here are fairly typical, and thus, the results showing lower viscosity/surface tension for laboratory particles compared to ambient particles are relevant for a wide range of laboratory studies.

Figure 3 shows the particle size as a function of the OD at the preedge, $OD_{278}$. The black data points are the combined ambient data, and the red data points are the combined laboratory-generated data. The slope of the best fit line for the ambient data is an order of magnitude higher than the slope for the laboratory-generated particles. The preedge absorbance is due to absorbance and scattering by atoms other than carbon such as O, N, S, etc. The difference in slopes indicates that the ambient particles have more heteroatoms than the laboratory-generated particles. For the ambient particles, the contribution from other absorbing and scattering elements was estimated by calculating the thickness ratio of organic to inorganic components using $OD_{278}$ and $OD_{320}$ measurements and estimates of the mass absorption coefficients and densities for both organic and inorganic species (for calculations see supporting information). Approximately 10–30% of the thickness for the particles is likely due to nonorganic molecules or atoms. The ambient particles likely contain either more organosulfates and organonitrates, inorganic species dispersed in the particles such as $(NH_4)_2SO_4$ and NaCl, or unresolved nanoparticles containing other elements commonly observed in atmospheric aerosols [*Moffet et al.*, 2010b].

There are numerous plausible reasons for the observed differences between laboratory-generated and ambient aerosols. Aerosols in smog chambers are more concentrated prompting smaller, semivolatile organic compounds (SVOC), which would normally exist in gaseous phase under typical ambient conditions, to partition in to the particles potentially resulting in more liquid-like particles. The semivolatile compounds may be lost during measurements since STXM is performed after pumping to vacuum, and the potentially larger amount of SVOC in the chamber experiments could make the particles more optically thin. Chamber particles have reacted for a shorter length of time than aerosols in the ambient environment [*Ng et al.*, 2010]. In the chamber experiments, only a single precursor was used, whereas ambient samples can have a wide range of precursors. Finally, no inorganic seeds were used in the chamber studies which may impact the chemical composition of the particles and ultimately the particle phase state. Our results demonstrate that the chemical compositions and potentially the reaction kinetics of laboratory aerosols differ significantly from those in the ambient environment.

## 4. Summary and Conclusions

We investigated the extent of deformation of impacted aerosol particles from both field campaigns and laboratory studies using STXM/NEXAFS analysis of the TCA and the size of the particles. Samples with steeper slopes on a plot of TCA versus size likely have higher viscosities/surface tensions. The technique used here does not differentiate between the effects of viscosity versus surface tension on the final shape of the impacted particle. Future work using aerosols generated from materials with known viscosity and known surface tension will be used to quantify the trends observed in this work.

The slopes for the ambient samples are all statistically similar. The laboratory-generated samples all had lower slopes than the ambient samples indicating lower viscosities/surface tensions than for particles measured during ambient field campaigns. The differences in aging time, aerosol mass concentration, volatility, number of precursors, and lack of any inorganic compounds in the laboratory samples likely contribute to these results. Since the viscosity will affect chemical diffusion rates and the surface tension will affect vapor pressures of the organic components in an aerosol particle, the lower viscosities/surface tensions in the laboratory samples can impact the kinetics of SOA formation, gas-particle partitioning, and the chemical composition of the laboratory-generated aerosols as compared to ambient aerosols. Thus, caution should be used when comparing the results of laboratory experiments to ambient samples and when applying data from laboratory studies to SOA models. The similarity in slopes between the ambient samples indicates that despite the different sources, meteorology, formation, and aging processes at the different field sites, a small range of viscosities/surface tensions may be appropriate to describe the average ambient aerosol population in SOA models.

**Acknowledgments**

Data supporting Figures 2 and 3 are available in Table S5 in the supporting information. This work was supported in part by the U.S. Department of Energy's Atmospheric System Research, an Office of Science, Office of Biological and Environmental Research program. STXM/NEXAFS was done at beamlines 5.3.2.2 and 11.0.2 at The Advanced Light Source at Lawrence Berkeley National Laboratory (LBNL) which are supported by the Director, Office of Science, Office of Basic Energy Sciences, (beamline 11.0.2 is also supported by the Division of Chemical Sciences, Geosciences, and Biosciences) of the U.S. Department of Energy under contract DE-AC02-05CH11231. M.K.G. and S.T.K. also acknowledge support from the Condensed Phase and Interfacial Molecular Sciences Program under the same contract. We wish to acknowledge the continued support of A.L.D. Kilcoyne and T. Tyliszczak. SEM imaging of particles was performed at Environmental Molecular Sciences Laboratory, a national scientific user facility sponsored by OBER at Pacific Northwest National Laboratory. PNNL is operated by the U.S. Department of Energy by Battelle Memorial Institute under contract DE-AC06-76RL0. The UCI team acknowledges support from the National Science Foundation grant CHE-0909227.

The Editor thanks two anonymous reviewers for their assistance in evaluating this paper.

## References

Abramson, E., D. Imre, J. Beránek, J. Wilson, and A. Zelenyuk (2013), Experimental determination of chemical diffusion within secondary organic aerosol particles, *Phys. Chem. Chem. Phys.*, *15*(8), 2983–2991.

Bones, D. L., D. K. Henricksen, S. A. Mang, M. Gonsior, A. P. Bateman, T. B. Nguyen, W. J. Cooper, and S. A. Nizkorodov (2010), Appearance of strong absorbers and fluorophores in limonene-$O_3$ secondary organic aerosol due to $NH_4^+$-mediated chemical aging over long time scales, *J. Geophys. Res.*, *115*, D05203, doi:10.1029/2009JD012864.

Cappa, C. D., and K. R. Wilson (2011), Evolution of organic aerosol mass spectra upon heating: Implications for OA phase and partitioning behavior, *Atmos. Chem. Phys.*, *11*(5), 1895–1911.

Hallquist, M., et al. (2009), The formation, properties and impact of secondary organic aerosol: Current and emerging issues, *Atmos. Chem. Phys.*, *9*(14), 5155–5236.

Hand, J. L., et al. (2005), Optical, physical, and chemical properties of tar balls observed during the Yosemite Aerosol Characterization Study, *J. Geophys. Res.*, *110*, D21210, doi:10.1029/2004JD005728.

Henke, B. L., E. M. Gullikson, and J. C. Davis (1993), X-Ray interactions: photoabsorption, scattering, transmission, and reflection at E = 50-30,000 eV, Z = 1-92, *At. Data Nucl. Data Tables*, *54*(2), 181–342.

Ivosevic, M., R. A. Cairncross, and R. Knight (2006), 3D predictions of thermally sprayed polymer splats: Modeling particle acceleration, heating and deformation on impact with a flat substrate, *Int. J. Heat Mass Transfer*, *49*(19–20), 3285–3297.

Kilcoyne, A. L. D., et al. (2003), Interferometer-controlled scanning transmission X-ray microscopes at the Advanced Light Source, *J. Synchrotron Radiat.*, *10*, 125–136.

Koop, T., J. Bookhold, M. Shiraiwa, and U. Poschl (2011), Glass transition and phase state of organic compounds: Dependency on molecular properties and implications for secondary organic aerosols in the atmosphere, *Phys. Chem. Chem. Phys.*, *13*(43), 19,238–19,255.

Kuwata, M., and S. T. Martin (2012), Phase of atmospheric secondary organic material affects its reactivity, *Proc. Natl. Acad. Sci. U.S.A.*, *109*(43), 17,354–17,359.

Laskin, A., J. P. Cowin, and M. J. Iedema (2006), Analysis of individual environmental particles using modern methods of electron microscopy and X-ray microanalysis, *J. Electron Spectrosc. Relat. Phenom.*, *150*(2–3), 260–274.

Loza, C. L., M. M. Coggon, T. B. Nguyen, A. Zuend, R. C. Flagan, and J. H. Seinfeld (2013), On the mixing and evaporation of secondary organic aerosol components, *Environ. Sci. Technol.*, *47*(12), 6173–6180.

Marple, V. A., K. L. Rubow, and S. M. Behm (1991), A microorifice uniform deposit impactor (MOUDI): Description, calibration, and use, *Aerosol Sci. Technol.*, *14*(4), 434–446.

Moffet, R. C., T. Henn, A. Laskin, and M. K. Gilles (2010a), Automated chemical analysis of internally mixed aerosol particles using X-ray spectromicroscopy at the carbon K-edge, *Anal. Chem.*, *82*(19), 7906–7914.

Moffet, R. C., et al. (2010b), Microscopic characterization of carbonaceous aerosol particle aging in the outflow from Mexico City, *Atmos. Chem. Phys.*, *10*(3), 961–976.

Moffet, R. C., A. V. Tivanski, and M. K. Gilles (2011), Scanning transmission X-ray microscopy applications in atmospheric aerosol research, in *Fundamentals and Applications in Aerosol Spectroscopy*, edited by R. Signorell and J. P. Reid, pp. 434–436, CRC Press, Taylor & Francis Group, Boca Raton, Fla.

Molina, L. T., et al. (2010), An overview of the MILAGRO 2006 Campaign: Mexico City emissions and their transport and transformation, *Atmos. Chem. Phys.*, *10*(18), 8697–8760.

Ng, N. L., et al. (2010), Organic aerosol components observed in Northern Hemispheric datasets from Aerosol Mass Spectrometry, *Atmos. Chem. Phys.*, *10*(10), 4625–4641.

Nguyen, T. B., J. Laskin, A. Laskin, and S. A. Nizkorodov (2011a), Nitrogen-containing organic compounds and oligomers in secondary organic aerosol formed by photooxidation of isoprene, *Environ. Sci. Technol.*, *45*(16), 6908–6918.

Nguyen, T. B., P. J. Roach, J. Laskin, A. Laskin, and S. A. Nizkorodov (2011b), Effect of humidity on the composition of isoprene photooxidation secondary organic aerosol, *Atmos. Chem. Phys.*, *11*(14), 6931–6944.

Pankow, J. F. (1994), An absorption-model of gas-particle partitioning of organic-compounds in the atmosphere, *Atmos. Environ.*, *28*(2), 185–188.

Perraud, V., et al. (2012), Nonequilibrium atmospheric secondary organic aerosol formation and growth, *Proc. Natl. Acad. Sci. U.S.A.*, *109*(8), 2836–2841.

Renbaum-Wolff, L., J. W. Grayson, M. Kuwata, A. P. Bateman, M. Sellier, B. J. Murray, J. Shilling, S. T. Martin, and A. K. Bertram (2013), Viscosity of alpha-pinene secondary organic material and implications for particle growth and reactivity, *Proc. Natl. Acad. Sci. U.S.A.*, *110*(20), 8014–8019.

Saukko, E., H. Kuuluvainen, and A. Virtanen (2012), A method to resolve the phase state of aerosol particles, *Atmos. Meas. Tech.*, *5*(1), 259–265.

Vaden, T. D., C. Song, R. A. Zaveri, D. Imre, and A. Zelenyuk (2010), Morphology of mixed primary and secondary organic particles and the adsorption of spectator organic gases during aerosol formation, *Proc. Natl. Acad. Sci. U.S.A.*, *107*(15), 6658–6663.

Vaden, T. D., D. Imre, J. Beránek, M. Shrivastava, and A. Zelenyuk (2011), Evaporation kinetics and phase of laboratory and ambient secondary organic aerosol, *Proc. Natl. Acad. Sci. U.S.A.*, *108*(6), 2190–2195.

Virtanen, A., et al. (2010), An amorphous solid state of biogenic secondary organic aerosol particles, *Nature*, *467*(7317), 824–827.

Wang, B. B., A. T. Lambe, P. Massoli, T. B. Onasch, P. Davidovits, D. R. Worsnop, and D. A. Knopf (2012), The deposition ice nucleation and immersion freezing potential of amorphous secondary organic aerosol: Pathways for ice and mixed-phase cloud formation, *J. Geophys. Res.*, *117*, D16209, doi:10.1029/2012JD018063.

Wood, R., et al. (2011), The VAMOS Ocean-Cloud-Atmosphere-Land Study Regional Experiment (VOCALS-REx): Goals, platforms, and field operations, *Atmos. Chem. Phys.*, *11*(2), 627–654.

Zaveri, R. A., et al. (2010), Nighttime chemical evolution of aerosol and trace gases in a power plant plume: Implications for secondary organic nitrate and organosulfate aerosol formation, $NO_3$ radical chemistry, and $N_2O_5$ heterogeneous hydrolysis, *J. Geophys. Res.*, *115*, D12304, doi:10.1029/2009JD013250.

Zaveri, R. A., et al. (2012), Overview of the 2010 Carbonaceous Aerosols and Radiative Effects Study (CARES), *Atmos. Chem. Phys.*, *12*(16), 7647–7687.

Zhang, Q., et al. (2007), Ubiquity and dominance of oxygenated species in organic aerosols in anthropogenically-influenced Northern Hemisphere midlatitudes, *Geophys. Res. Lett.*, *34*, L13801, doi:10.1029/2007GL029979.